ISES International Solar Energy Society

Conference Proceedings

EuroSun 2014
Aix-les-Bains (France), 16 – 19 September 2014

Experimental and Numerical Investigation of a Packed-Bed Latent Heat Thermal Storage System with Encapsulated Phase Change Material

Tanvir E Alam[1], Selvan Bellan[2], Jaspreet Dhau[3,4], D. Y. Goswami[4,5], M.M. Rahman [1,4] , E. Stefanakos[3,4] Jose Gonzalez-Aguilar [2], Manuel Romero [2].

[1] Department of Mechanical Engineering, University of South Florida, Tampa, Florida, USA.

[2] IMDEA Energy Institute, Ramon de la Sagra 3, 28935 Móstoles, Spain.

[3] Department of Electrical Engineering, University of South Florida, Tampa, Florida, USA.

[4] Clean Energy Research Center, University of South Florida, Tampa, Florida, USA.

[5] Department of Chemical & Biomedical Engineering, University of South Florida, Tampa, Florida, USA.

Abstract

A laboratory scale packed bed latent heat thermal energy storage (TES) system was designed and built to study its charging and discharging behavior. Encapsulated sodium nitrate spherical capsules were used as the storage material and air was used as the heat transfer fluid. A two-dimensional two-phase model was developed by assuming that the PCM capsules behave as continuous, homogeneous, and isotropic porous medium, and not as a medium composed of independent particles. The heat transfer coefficient was calculated based on the phase change process inside the capsule by enthalpy formulation model. The flow inside the system was predicted by solving the extended Brinkman equation. The developed model was used to analyze the temperature distribution inside the capsules placed at different axial positions of the bed. The effect of mass flow rate on the charging and discharging times and melt fraction of the packed bed during the charge and discharge processes were also analyzed. The results obtained from the model matched well with the experimentally observed results.

Keyword: Phase change material, Packed-bed latent heat Storage, Encapsulated capsule

1. Introduction

Even though, we have an abundance of solar energy; intermittency of the resource poses a big problem for continuous use. Integration of thermal energy storage with solar energy systems could be a viable solution to this problem, especially in CSP plants [1, 2]. Among the thermal energy storage (TES) techniques, latent heat thermal storage (LHTS) can provide higher storage density than the sensible heat storage that substantially reduces the size of the storage tank and the associated equipment leading to a significant reduction in the capital costs [3-5]. In spite of these benefits, latent heat based storage systems have not been commercially exploited in solar power plants. One of the major reasons is inefficient energy retrieval from the bulk system due to low thermal conductivity of the PCMs [6, 7]. Different methods have been proposed and explored to enhance the thermal conductivity of the PCMs such as addition of highly conductive nano or expanded graphite mixture [8, 9], insertion of metal particles into the PCM matrix, use of extended surface (fin) [10], and shell and tube heat exchanger [11]. Other methods include micro- and macro-encapsulation of the PCMs to reduce the path length for heat transfer [12-15].

Many research groups have shown interest in Macro-encapsulated spherical PCMs capsule in a packed- bed storage system [16-28]. Regin et al. [17] presented a review of the encapsulated PCMs, and their application in latent heat thermocline systems and also developed a numerical model of a paraffin wax based system [18]. Saitoh and Hirose [19] experimentally and analytically discussed spherical capsules of different diameter and HTF flow rate and their influence on overall heat transfer rate. Ozturk [20] worked with

Selection and/or peer review under responsibility of EuroSun2014 Scientific Committee
doi:10.18086/eurosun.2014.10.01 Available at http://proceedings.ises.org

paraffin as the PCM to experimentally investigate the thermal effect of LHTS on greenhouse heating. Michels and Pitz-Paal [21] reported an experimental and numerical investigation on a cascaded latent heat thermal storage system with alkali metal nitrate PCMs. Recently, Esakkimuthu et al. [22], Xiao and Zhang [23] performed experiments with low-temperature organic PCMs. They have investigated the performance characteristics of a LHTS packed bed system. Archibold et al. [24] numerically investigated the heat transfer performance and fluid flow during melting inside a spherical container for TES. They demonstrated the melting dynamics of capsules of different diameters. A survey of the literature reveals only a few reports on the high-temperature numerical analysis of LHTS. Bellan et al.[25] developed a transient numerical model for an encapsulated $NaNO_3$ PCM based LTHS system and optimized the main parameters of storage tanks. Peng et al. [26] performed a numerical analysis of an LTHS system containing a high-temperature PCM ($NaNO_2$). They examined the temperature distribution inside the bed and established the relationships of charging and discharging efficiencies with flow rate and capsule size. Nithyanandam et al. [27] also built a model to analyze a latent heat thermocline storage system with encapsulated PCMs and proposed guidelines for designing a PCM based packed bed system.

It is evident from the above literature review that there is no experimental demonstration of the packed-bed LHTS system available on high temperature (>300°C) encapsulated PCMs. This is in part due to non-availability of any technique to encapsulate PCM on a large scale. We have successfully developed a non-vacuum encapsulation technique that can fabricate encapsulated spherical high-temperature PCM capsules on large scale. The encapsulated PCM capsules developed by this technique have survived more than 2200 thermal cycles without any failure. The objective of the present study was to develop a lab scale LHTS system containing sodium nitrate ($NaNO_3$) capsules and air as the heat transfer fluid (HTF). We have also developed a two-dimensional two-phase model that was used to analyze the temperature profiles of the PCM capsules at various axial positions of the storage tank and at three different flow rates. The influence of the flow rate of HTF over the charging and discharging times, melt fraction and solid faction of the bed was also investigated. The developed model was validated by the experimentally observed results.

2. Experimental Setup

The experimental packed bed setup consists of a blower, a cylindrical tank, electrical heaters, and flow measuring device (pitot tube). A schematic of the setup is illustrated in Fig. 1.

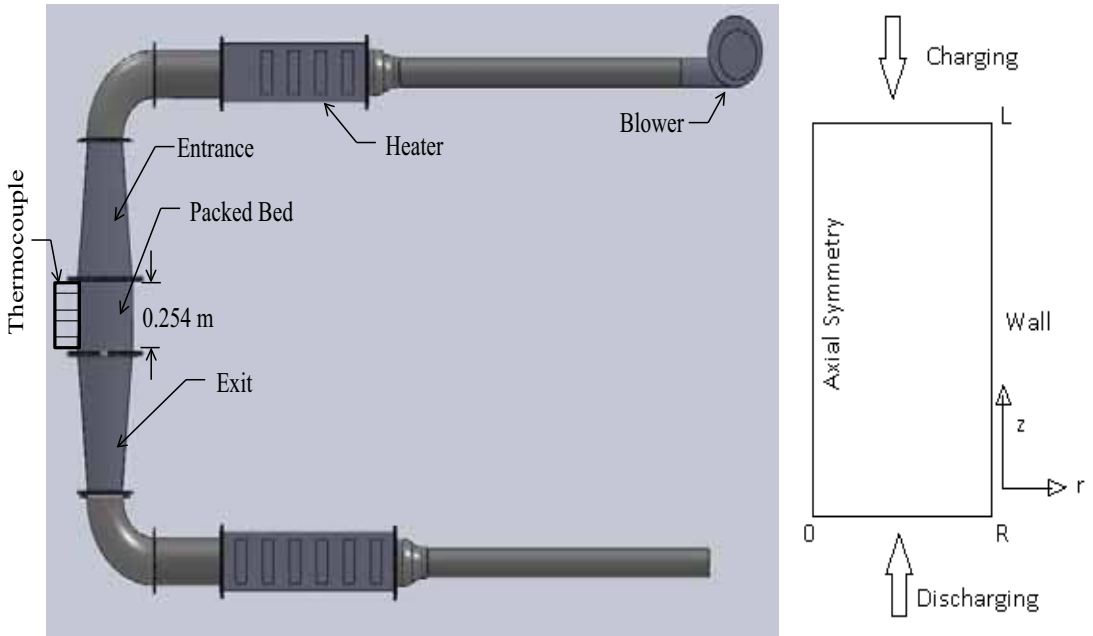

Figure 1: Schematic of the experimental setup (left hand side) and computational domain (right hand side)

The construction material of the storage tank is carbon steel of 0.254 m (10 inches) height and diameter. The whole system was well-insulated with thermal insulation of 0.1524 m thickness. The packed-bed was randomly packed with 770 encapsulated spherical $NaNO_3$ capsules. The average diameter and volume of the capsules are 2.743±0.038 cm and 10.39±0.21 cm^3, respectively. The average porosity of the bed and bed-to-particle diameter were fixed at 0.35 and 10, respectively.

In total, 24 K-type thermocouples were installed along the axial and radial directions of the bed and two thermocouples were used after the heaters. Axially, thermocouples were installed 0.0508 m apart from each other, divided into four rows across the length of the bed starting from the top. Thermocouples were also fitted inside some of the centrally placed capsules that are axially 0.0508 m apart from each other. One thermocouple was installed at 0.0254 m above the top of the bed to measure the inlet (charging) temperature of the bed. Another thermocouple was installed at 0.0254 m below the bottom of the bed to measure the outlet (charging) temperature of the bed.

Air flow in the system was produced by a centrifugal blower and six heaters were used to heat the entering the bed. Figure 2 shows the complete experimental setup.

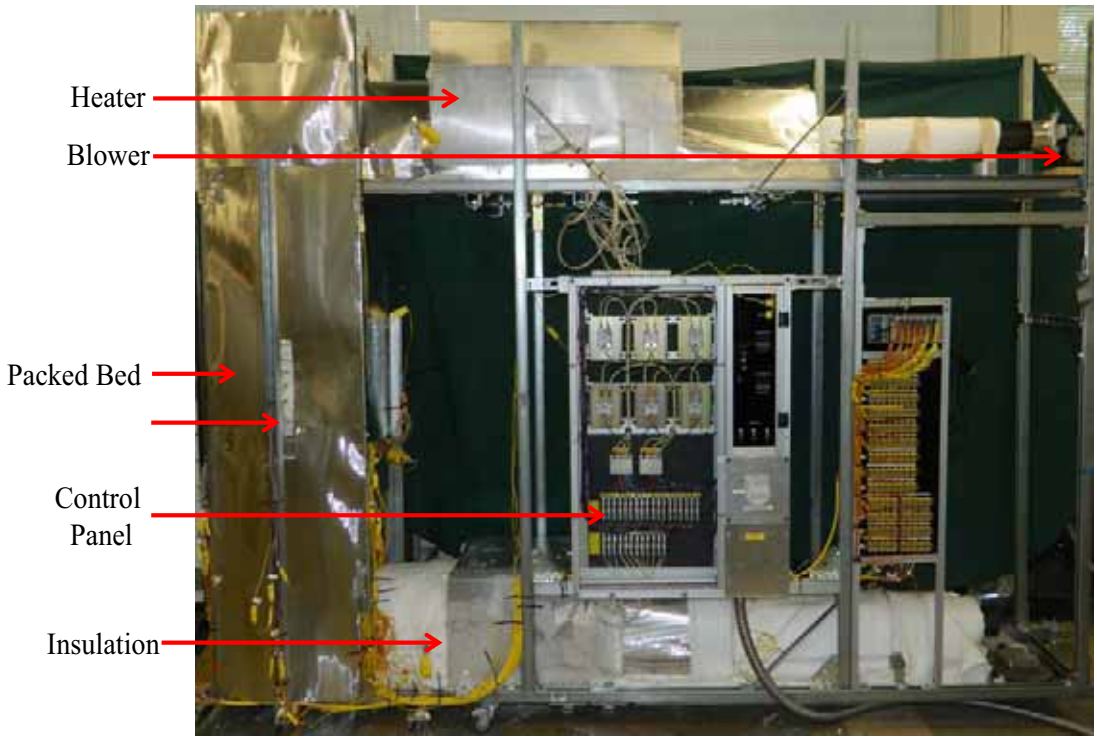

Figure 2: Complete experimental setup

Before charging, the air-blower was connected to the top side of the packed-bed system. The whole system was heated to 286°C and maintained at this temperature. For the charging of the system, the inlet temperature of the HTF was increased to 326°C. Charging was complete when the whole TES system reached 326°C. For the discharging step, the blower from the top was moved down and connected with the bottom heater which heated the HTF to 286°C before entering the system. As the system temperature decreases from 326°C to 286°C, the discharging step was considered to be complete. Testing of the system was performed at three different flow rates (Table 1). Temperature data were collected by Labview Express at 60 sec interval.

Table 1: Operation parameters

case	Flow rate (m^3/hr)	Charging temperature (°C) (Bed initially at 286°C)	Discharging temperature (°C) (Bed Initially at 326°C)
1	110	326	286
2	131	326	286
3	151	326	286

3. Numerical Modelling

The schematic of the computational domain is shown in Fig.1. The numerical model is developed based on the following assumptions:

(1) The thermo-fluid flow is assumed as symmetrical about the axis. Thus, the governing equations for heat transfer and fluid flow within the storage tank become two-dimensional.

(2) The flow is laminar and incompressible.

(3) The PCM capsules behave as a continuous, homogeneous and isotropic porous medium.

(4) The radiation heat transfer between the capsules is negligible.

(5) The rhombic packing is assumed; the distribution of spherical capsules inside the tank is defined by the porosity (ε), as given below [16].

$$\varepsilon(r) = \varepsilon_{avg}\left[a_1 + \left(\frac{a_2}{\varepsilon_{avg}} - 1\right)\exp\left(-a_3\frac{R-r}{d}\right)\right] \quad \text{(eq. 1)}$$

where, ε_{avg} and d are the average porosity and diameter of the capsule respectively. The average porosity is 0.3446, and the empirical constants a_1, a_2 and a_3 are 0.955, 0.7 and 10 respectively. These values are found to be a good approximation to the experimental data. By assuming the above points, the system of the governing equations to simulate the fluid flow and heat transfer inside the tank are given as follows:

Continuity equation

$$\rho\nabla.V = 0 \quad \text{(eq. 2)}$$

Momentum equation

$$\frac{\rho_f}{\varepsilon}\left(\frac{\partial V}{\partial t} + (V.\nabla)\frac{V}{\varepsilon}\right) = -\left(\frac{\mu}{K} + F(V)\right)V + \frac{\mu}{\varepsilon}\nabla^2(V) - \nabla(P) \quad \text{(eq. 3)}$$

Where ρ, μ, V and P are density, viscosity, velocity vector and pressure respectively. The permeability of the porous medium K and the Forchheimer coefficient are given as [28].

$$K = \frac{\varepsilon^3 d^2}{150(1-\varepsilon)^2} \quad \text{(eq. 4)}$$

$$F = \frac{\rho_f \varepsilon}{\sqrt{K}}\left(\frac{1.75}{\sqrt{150\varepsilon^3}}\right) \quad \text{(eq.5)}$$

Energy equation

HTF energy equation

$$\varepsilon(\rho c_p)_f \frac{\partial T_f}{\partial t} + (\rho c_p)_f V.\nabla T_f) = \nabla.(k_{f\,eff}\nabla T_f) + Ua_p(T_s - T_f) \quad \text{(eq. 6)}$$

PCM energy equation

$$(1-\varepsilon)(\rho c_p)_s \frac{\partial T_s}{\partial t} = \nabla.(k_{s\,eff}\nabla T_s) + Ua_p(T_f - T_s) \quad \text{(eq. 7)}$$

where T_f and T_s represent the temperature of the heat transfer fluid and PCM capsules respectively, c_p is specific heat capacity, U is the overall heat transfer coefficient, and a_p is the superficial particle area per unit bed volume which is given by

$$a_p = \frac{6(1-\varepsilon)}{d} \quad \text{(eq. 8)}$$

Effective thermal conductivities $k_{f\,eff}$ and $k_{s\,eff}$ are given by

$$k_{f\,eff} = \varepsilon k_f \quad \text{(eq. 9)}$$

$$k_{s\,eff} = (1-\varepsilon)k_s \quad \text{(eq. 10)}$$

The last term on the right-hand side of the energy equation, which accounts for the heat transfer between the PCM capsules and HTF, plays a vital role in the thermal performance of the system. Hence, the overall heat transfer coefficient (U) is calculated according to the packed-bed configuration, and the thermal resistance concept, which is described in [25, 29].

Table 2. Thermophysical properties of sodium nitrate

Properties	Sodium Nitrate
Density (kg/m^3)	
solid phase	2130
mushy zone	*Linear interpolation*
liquid phase	1908
Dynamic viscosity (Pa s)	$0.0119 - 1.53x10^{-5}T$
Latent heat of fusion (J/kg)	178000
Melting temperature (°C)	306.8
Specific heat (J/kg/K)	$444.53 + 2.18T$
Thermal expansion coef.(K^{-1})	$6.6x10^{-4}$
Thermal conductivity (W/m/K)	$0.3057 + 4.47x10^{-4}T$

In this investigation, the spherical capsule contains $NaNO_3$ in a polymer shell of thickness = 0.41 mm. The temperature dependent thermo-physical properties of $NaNO_3$ are given in Table 2. The thermal resistance caused by the shell is included in the model. Thermal conductivity of the polymer is 0.25Wm^{-1}K^{-1}. The boundary conditions are given in Table 3. The melting of the PCM is assumed between T_{sol}= 305 ºC and T_{liq} = 307ºC (mushy zone). Hence, the melt fraction, γ, at each element of the PCM domain is given by

$$\gamma = \begin{cases} 0 & if\ T_s < T_{sol} \\ \dfrac{T_s - T_{sol}}{T_{liq} - T_{sol}} & if\ T_{sol} \le T_s \le T_{liq} \\ 1 & if\ T_s > T_{liq} \end{cases} \quad \text{(eq. 11)}$$

Table 3. Boundary conditions.

Boundary	HTF	PCM
Inlet	$T_f(t)$	$\partial T_s / \partial z = 0$
Outlet	$\partial T_f / \partial z = 0$	$\partial T_s / \partial z = 0$
Wall	$U_w(T_a - T)$	$\partial T_s / \partial r = 0$
Axial symmetry	$\partial T_f / \partial r = 0$	$\partial T_s / \partial r = 0$

4. Model Validation

Experiments were carried out under the operating parameters given in Table 1. Simulations were performed for various transition (phase change range) points, such as (305-307 ºC), (306-308 ºC), (307-309 ºC), for case

1. Fig. 3 shows the temperature distribution of the PCM during the discharge process, at z/L= 0.8, for various transition points along with the experimentally measured temperatures. The error analysis of temperature measurements is made with 95% confidence intervals and shown in the figure. It is noticed that the phase change range (305-307 ºC) provides the temperature distribution close to the experimental results. Hence, by assuming the melting range is between 305 and 307 ºC (mushy zone) simulations were performed for various gas flow rates (Refer Table 1).

Experimentally measured and numerically predicted PCM temperature distributions at two axial positions during charging and discharging modes are compared in Fig. 4. It is observed that the numerical results are comparable with the experimental results. The maximum difference between the predicted and numerical results is near the phase change range.

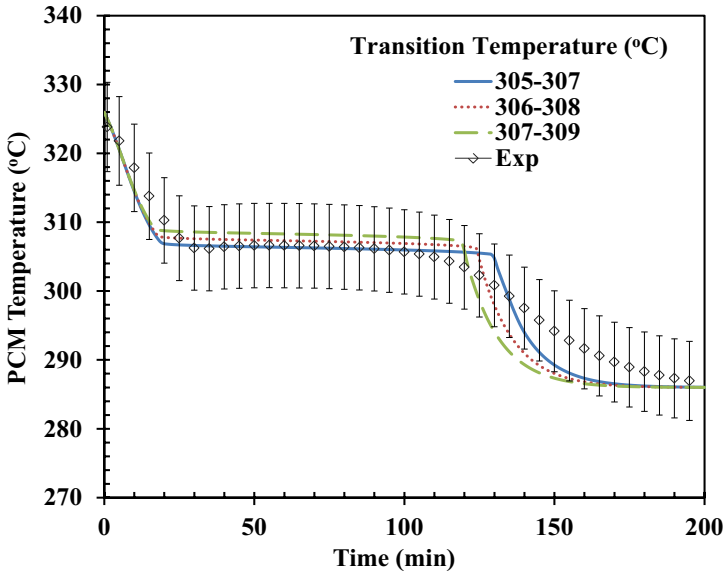

Fig. 3. Temperature distribution of the PCM at z/L=0.8 for various transition temperatures

Fig. 5 shows the charging time of the PCM at various heights of the bed measured experimentally, and also using the developed model for three different mass flow rates. The charging time refers to the time required for the PCM at a given height, to attain the temperature of the inlet HTF. It is seen from the figure that the predicted results are in good agreement with the results of the experiments in all cases. Moreover, the developed model was extensively validated with various experimental studies [29].

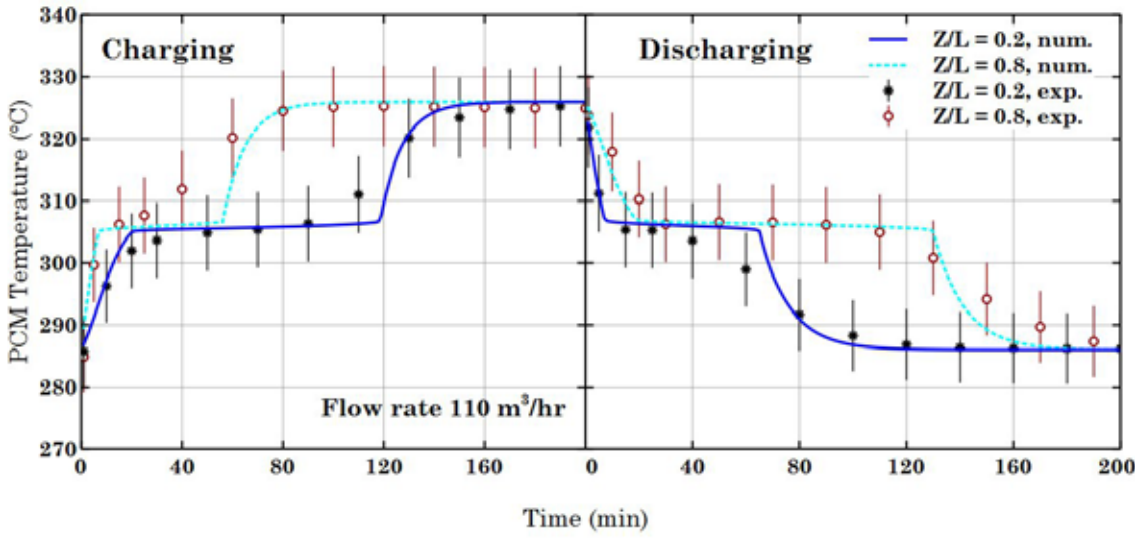

Fig. 4. Experimentally measured and numerically predicted PCM temperature distributions at two axial positions during charging and discharging modes.

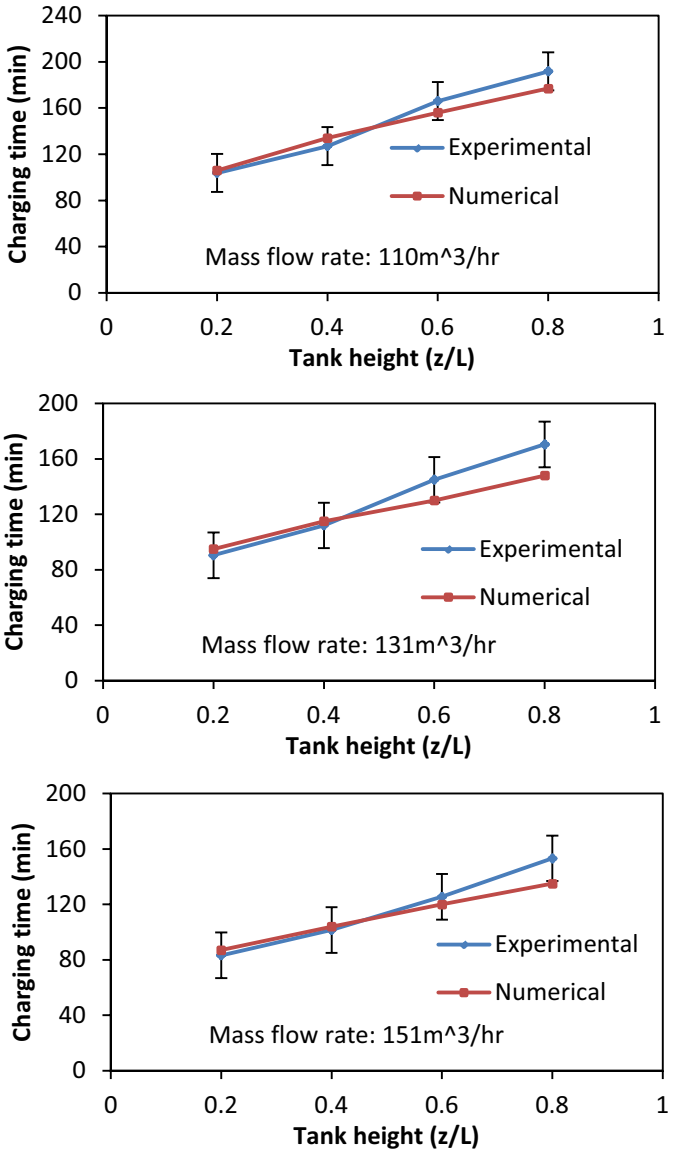

Fig.5. Charging time of PCM at various height of the bed for various flow rates. (Uncertainty of the charging time is ±16.45 min)

5. Uncertainty Analysis

Experiments were conducted several times to observe the repeatability of the measured data. The Root-sum-square method was used to determine the uncertainty of the measurements [30]. The error calculations were computed within 95% of confidence level. The Uncertainty associated with the flow rate and temperature measurements were 5.78% and 2.19%, respectively.

$$U_c = \sqrt{((\sigma_{random})^2 + (\sigma_{systematic})^2)} \quad \text{(eq. 12)}$$

Where, U_c, σ_{random} and $\sigma_{systematic}$ are combined standard uncertainty, random error and systematic error respectively.

6. Results and Discussion

The temperature distribution of the PCM at various axial locations are predicted for various cases and shown in Fig. 6. It shows that for a fixed flow rate, the charging time of the system was less than the discharging time. This is because the melting process is a natural convection dominated process where solidification is a conduction dominant process. It was also observed that with the increase in the flow rate, the charging and discharging times decrease.

The melt fraction of the packed bed during the charging and discharging processes are shown in Fig. 7 (a) and (b) respectively as a function of time for various HTF flow rates. As expected, the complete melting/solidification times of the tank are decreased when the fluid flow rate is increased, due to the heat transfer rate. Difference between the complete melting and solidification times is noticed.

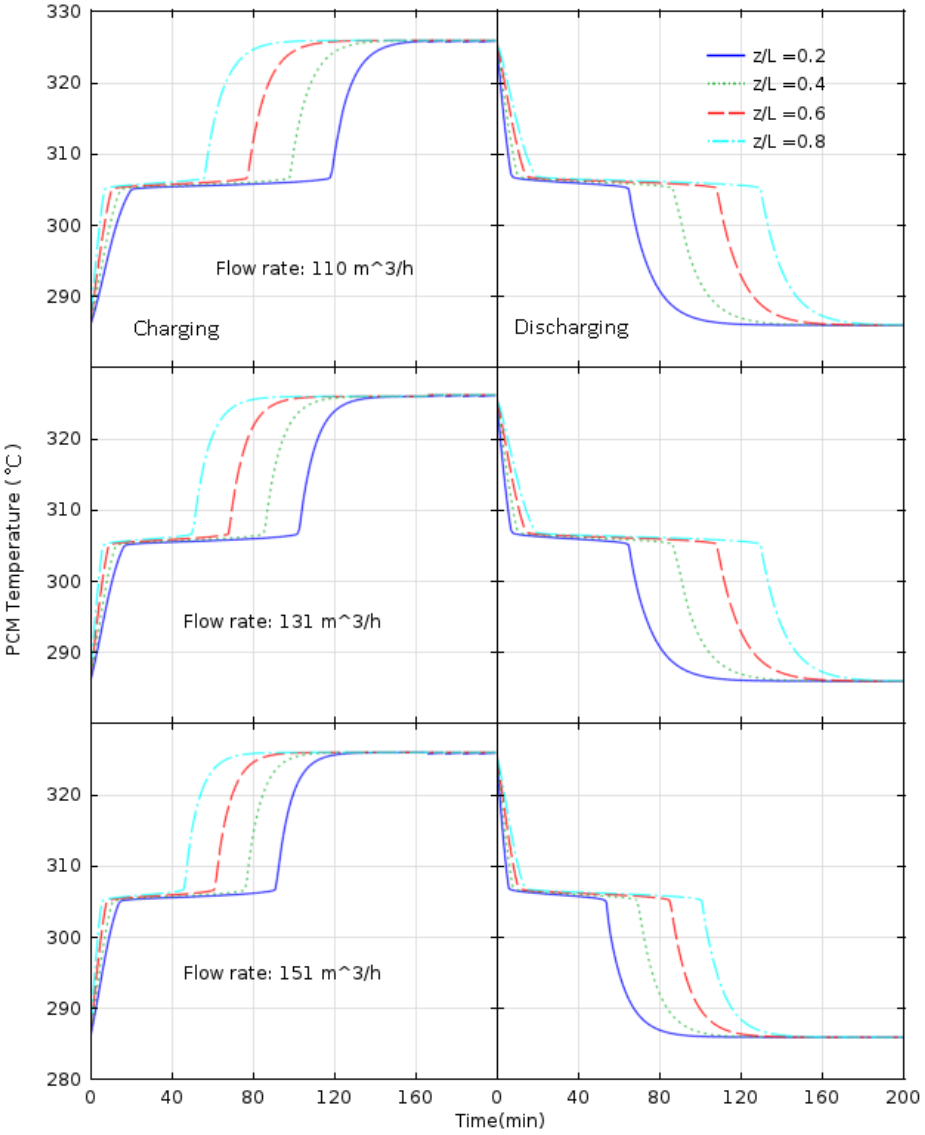

Fig. 6. Temperature distribution of the PCM at various axial locations during charging and discharging processes for various HTF flow rates.

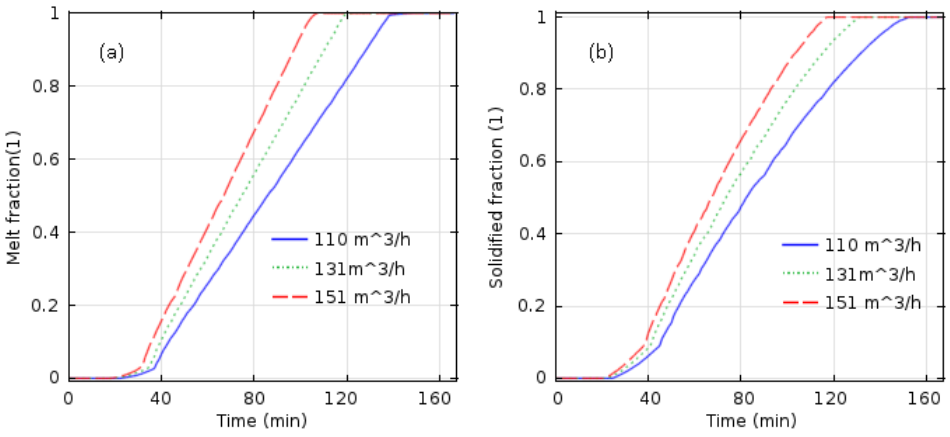

Fig.7 (a) Melt fraction and (b) solidified fraction of the bed during charge and discharge processes for various HTF flow rates.

7. Conclusion

An experimental investigation was conducted on a high-temperature LHTS system using encapsulated $NaNO_3$ spherical capsules and air as the HTF. A transient two-dimensional two-phase model for spherical encapsulated PCM capsules was developed and validated with the experimental results. The model shows good agreement with the experimental results. Temperature profile of the PCM capsules at various axial positions of the storage was predicted. Flow rate has an influence on the heat transfer process. With the increase in the HTF flow rate, decrease in the complete melting/solidification time of the tank is observed. Also, it is observed that the melting time is shorter than the solidification time due to the heat transfer coefficient during melting.

8. Acknowledgement

This research is partially supported by US Department of Energy (#2131100900) and E-ON Corporation (#2131100900) through a research project entitled “Innovative latent Thermal Energy Storage System for Concentrating Solar Power Plants”.

9. References

[1] Zalba, B., Marín, J.M., Cabeza, L.F., Mehling H., 2003. Review on Thermal Energy Storage with Phase Change: Materials, Heat Transfer Analysis and Applications. Applied Thermal Engineering. 23(3), 251-283.

[2] Kuravi, S., Trahan, J., Goswami, D.Y., Rahman, M.M., Stefanakos, E.K., 2013.Thermal Energy Storage Technology and Systems for Concentrating Solar Power plants. Progress in Energy and Combustion Science. 39(40), 285-319.

[3] Kaya, G., Laby, T., 1986. Tables of Physical and Chemical Constants and Some Mathematical Functions. Longman, London,UK.

[4] Hasnain, S.M., 1998. Review on Sustainable Thermal Energy Storage Technology, Part 1: Heat Storage Materials and Techniques. Energy Conversion and Management. 39(11), 1127-1138.

[5] Ibrahim, D, March, R., 2002. Thermal Energy Storage. Wiley, New York.

[6] Kenisarin, M.M., 2010.High Temperature Phase Change Materials for Thermal Energy Storage. Renewable and Sustainable Energy Reviews. 14(3), 955-970.

[7] Lui, M., Saman, W., Bruno, F., 2012. Review on Storage Materials and Thermal Performance Enhancement techniques for High Temperature Phase Change Thermal Storage System. Renewable and Sustainable Energy Reviews. 16(4),2118-2132.

[8] Kumaresan, V., Velraj, R., Das, S.K., 2012. The Effect of Carbon Nanotubes in Enhancing the Thermal Transport Properties of PCM During Solidification. Heat and Mass Transfer. 48 (8), 1345-1355.

[9] Xiao, X., Zhang, P., Li, M., 2013.Thermal Characterization of Nitrates and Nitrates/Expanded Graphite Mixture Phase Change Materials for Solar Energy Storage. Energy Conversion and Management. 73, 86-94.

[10] Laing, D., Bauer, T., Breidenbach, N., Hachmann, B., Johnson, M., 2013. Development of High Temperature Phase Change material Storages. Applied Energy. 109, 497-504.

[11] Tao, Y.B., He Y.L., 2011. Numerical Study on Thermal energy Storage Performance of Phase Change Material Under Non-Steady-State Inlet Boundary. Applied Energy. 88(11), 4172-4179.

[12] Sari, A., Alkan, C., Karaipekli, A., Uzun, O.,2009. Microencapsulated n-octacosane as Phase Change Material for Thermal Storage. Solar Energy. 83(10), 1757-1763.

[13] Hawlader, M.N.A., Uddin, M.S., Khin, M.M., 2003. Microencapsulated PCM Thermal Energy Storage System. Applied Energy. 74(1-2), 195-202.

[14] Mathur, A., (MN ,Shoreview), Kasetty, R. B., (CA Riverside), 2011. Thermal Energy Storage System Comprising Encapsulated Phase Change Material. United States of America Application No.- 61366409.

[15] Platte, D., Helbig, U., Houbertz, R., Sextl, G., 2013. Microencapsulation of Alkaline Salt Hydrate Melts for Phase Change Applications by Surface Thiol-Michael Addition Polymerization. Macromolecular Materials and Engineering. 298(1), 67-77.

[16] Arkar, C., Medved, S., 2005. Influence of accuracy of thermal property data of phase change material on the result of numerical model of packed bed latent heat storage with spheres. Thermochemica Acta. 438, 192-201.

[17] Regin, A.F., Solanki, S.C., Saini, J.S., 2008. Heat Transfer Characterstics of Thermal Energy Storage using spherical capsules: A Review. A Renewable & Sustainable Energy Reviews. 12, 2338-2458.

[18] Regin, A.F., Solanki, S.C., Saini, J.S., 2009. An Analysis of a Packed Bed Latent heat Thermal Energy Storage System Using PCM Capsules: Numerical Investigation. Renewable Energy. 34, 1765-1773.
[19] Saitoh, T., Hirose, K., 1986. High Performance Phase change Thermal Energy Storage using spherical capsules. Chemical Engineering Communications. 41(1-6), 39-58.
[20] Ozturk, H.H., 2005. Experimental Evaluation of Energy and Exergy Efficiency of a Seasonal Latent Heat Storage System for Greenhouse Heating. Energy Conversion and Management. 46(9-10), 1523–1542.
[21] Michels, H., Pitz-Paal, R., 2007. Cascaded Latent Heat Storage for Parabolic Trough Solar Power Plants. Solar Energy. 81, 829-837.
[22] Esakkimuthu, S., Hassabou, A.H., Palaniappan, C., Spinnler, M, Blumenberg, J,. Velraj, R., 2013 Experimental Investigation on Phase Change Material Based Thermal Storage System for Solar Air Heating Applications. Solar Energy. 88, 144-153.
[23] Xiao, X., Zhang, P., 2014. Experimental Investigation on Heat Storage/Retrieval Characteristics of A Latent Heat Storage System. Heat Transfer Engineering. 35(11-12), 1084-1097.
[24] Archibold,, A.R., Rahman, M. M., Goswami, D.Y., Stefanakos, E. K., 2014. Analysis of Heat Transfer and Fluid Flow During Melting Inside A Spherical Container for Thermal Energy Storage. Applied Thermal Engineering. 64 (1–2), 396-407.
[25] Bellan, S., Aguilar, J.G., Romero, M., Rahman, M.M., Goswami, D.Y., Stefanakos, E.K., 2013. Numerical Analysis of Packed bed Thermal Energy Storage System for Concentrating Solar Power Plants. ISES Solar World Congress , Cancun, Mexico.
[26] Peng, H., Dong, H., Ling, X., 2014. Thermal investigation of PCM-Based High Temperature Thermal energy Storage in Packed bed. Energy Conversion and Management. 81, 420-427.
[27] Nithyanandam, K., Pitchumani., R., Mathur, A., 2014. Analysis of A Latent Thermocline Storage System with Encapsulated Phase Change Materials For Concentrating Solar Power. Applied Energy. 113, 1446-1460.
[28] Alazmi, B., Vafai, K., 2002. Constant Wall Heat Flux Boundary Conditions in Porous Media Under Local Thermal Non-Equilibrium Conditions. International Journal of Heat and Mass Transfer. 45, 3071–3087.
[29] Bellan, S., Aguilar, J.G., Romero, M., Rahman, M.M., Goswami, D.Y., Stefanakos, E.K., Couling, D., 2014. Numerical Analysis of Charging and Discharging Performance of A Thermal Energy Storage System With Encapsulated Phase Change Material. Applied Thermal Engineering. 71, 481-500.
[30] Wheeler, A.J., Ganji, A. R., 2009. Introduction to Engineering Experimentation, Prentice Hall.